Green synthesis of Ag_2O nanoparticles using *Punica granatum* leaf extract for sulfamethoxazole antibiotic adsorption: characterization, experimental study, modeling, and DFT calculation

Noureddine El Messaoudi (noureddine.elmessaoudi@edu.uiz.ac.ma)
Ibn Zohr University: Universite Ibn Zohr https://orcid.org/0000-0003-2762-1395
Abdelaziz El Mouden
Ibn Zohr University: Universite Ibn Zohr
Yasmine Fernine
Sidi Mohamed Ben Abdellah University: Universite Sidi Mohamed Ben Abdallah
Mohammed El Khomri
Ibn Zohr University: Universite Ibn Zohr
Amal Bouich
Polytechnic University of Valencia: Universitat Politecnica de Valencia
Nadia Faska
Ibn Zohr University: Universite Ibn Zohr
Zeynep Ciğeroğlu
Usak University: Usak Universitesi
Juliana Heloisa Pinê Américo-Pinheiro
Brazil University: Universidade Brasil
Amane Jada
Higher Alsace University: Universite de Haute-Alsace
Abdellah Lacherai
Ibn Zohr University: Universite Ibn Zohr

Research Article

Keywords: Sulfamethoxazole removal, green synthesis, Ag2O nanoparticles, kinetics and isotherm, DFT calculation

Posted Date: June 9th, 2022

DOI: https://doi.org/10.21203/rs.3.rs-1642752/v1

Abstract

In this study, silver oxide nanoparticles (Ag_2O NPs) were generated by synthesizing green leaf extract of *Punica granatum* and used as adsorbent and used as adsorbent to remove the antibiotic additive sulfamethoxazole (SMX) from an aqueous solution. The chemical composition, surface morphology, and textural properties of the Ag_2O NPs were identified using XRD, FTIR, BET/BJH, SEM-EDX, and TEM analyses. For 100 mg L^{-1} SMX antibiotic concentration, Ag_2O NPs achieved almost complete removal of 98.93% within 90 min by using 0.8 g L^{-1} of adsorbent dose and initial solution pH of 4 at a temperature of 308 K. Langmuir model efficiently elucidates the experimental data, which amounts to homogeneous nature of antibiotic adsorption onto the Ag_2O NPs. The maximum uptake capacity was 277.85 mg g^{-1}. Kinetic studies promise a PSO model. The ΔG^o and ΔH^o values confirm the spontaneity and endothermicity of the adsorption process. The regeneration study shows that the Ag_2O NPs can be efficiently reused for up to five cycles. The geometric structures have been optimized and quantum chemical parameters were calculated for the SMX unprotonated ($SMX^{+/-}$) and protonated (SMX^{+}) using density functional theory (DFT) calculation, indicating that the $SMX^{+/-}$ is reacting more favorably on the surface of Ag_2O NPs compared to the SMX^{+}. According to this study, the Ag_2O NPs as an excellent potential the adsorbent will be able to have remarkable effects in the treatment of pharmaceutical wastewater.

1 Introduction

The main source of water pollution is the direct discharge of wastewater into water bodies without any prior treatment (El Messaoudi et al. 2021a). Among the water pollutants, antibiotics, when released, pose serious threats even in small quantities. Antibiotics are chemical compounds that have the ability to inhibit the life processes of selected microorganisms (Khameneh et al. 2019). Antibiotics can be classified based on several factors such as chemical structure, method, etc. mode of action, the spectrum of action, and route of administration (injection, oral and topical). One of the best-known, perhaps simplest, classifications of antibiotics is based on the presence of distinct functional groups, such as macrolides, tetracyclines, quinolones, sulfonamides, oxazolidinones, etc. (Suzuki and Hoa 2012; Berges et al. 2021; Grenni 2022). Sulfonamides have been widely approved and used to treat a wide range of different clinical infections. They have been used for decades due to their high potency, broad-spectrum activity, and high serum concentrations (Fair and Tor 2014; Wang et al. 2019). Sulfamethoxazole (SMX) is a synthetic veterinary drug with a para-aminobenzene sulfonamide structure (Cheong et al. 2020). As a bacteriostatic sulfonamide antibiotic, SMX is used for the treatment and prevention of diseases in animals and humans (Zhang et al. 2011; Chen et al. 2017; Gao et al. 2019). Exposure of SMX to the environment can cause severe toxicity to be aquatic and nearby systems, bacteria, animals, and human health (Straub et al. 2016; Hwang et al. 2016; Xu et al. 2022). Therefore, the presence of antibiotics in water is unacceptable and there are currently several techniques to remove them, such as biodegradation, membrane separation, hydrolysis, and photodegradation (Mitchell et al. 2014; Reis et al. 2020; Wu et al.

2021; Yin et al. 2021). However, most of these techniques are still expensive, especially when applied to large quantities of industrial wastewater. Adsorption is one of the widely used and cost-effective techniques to remove pollutants from wastewater (El Khomri et al. 2021).

Multiple adsorbents such as graphene oxide (Chen et al. 2015), $CuZnFe_2O_4$/biochar (Heo et al. 2019), high silica zeolite Y (Braschi et al. 2016), waste-based activated carbon (Jaria et al. 2021), calcined layered double hydroxide (Mourid et al. 2019), zeolite (Liu et al. 2020a), sediment (Wang et al. 2017), and magnetic activated carbon (Lv et al. 2021), have been used for sulfamethoxazole (SMX) liquid phase remediation.

In recent years, green nanoparticles (ZnO, MgO, Fe_2O_3, Ag_2O, CuO, Si_2O, etc.) synthesized from extracts of lignocellulosic biomass have emerged as a cost alternative and are attractively low for cost-prohibited commercial NPs to reduce pollution as they promise effective adsorption due to their high efficiency, surface chemistry, porosity, selectivity, and surface chemistry (Ehrampoush et al. 2015; Stan et al. 2017; Asghar et al. 2018; Khani et al. 2018; SI et al. 2020; Pai et al. 2021). Compared with other synthesis methods (sol-gel, hydrothermal, precipitation, ultrasound, etc.), green synthesis of silver oxide nanoparticles (Ag_2O NPs) is simple, inexpensive, non-toxic, and environmentally friendly (Shamaila et al. 2016; Marouzi et al. 2021).

The present study is regarding the green synthesis of Ag_2O nanoparticles extracted from *Punica granatum* leaves and their evaluation by the adsorption of the sulfamethoxazole antibiotic from an aqueous solution. Additionally, the developed adsorbent was characterized using scanning electron microscopy/energy-dispersive X-ray (SEM/EDX), N_2 adsorption-desorption, X-ray diffraction (XRD), Fourier transform infrared (FTIR) spectroscopy, and transition electron microscopy (TEM) analyses. The effects of five independent active variables (pH, adsorbent dose, contact time, antibiotic concentration, and temperature) and their interactions on the adsorption capacity to remove SMX were examined. Kinetics (PFO, PSO, and IDP), equilibrium (Langmuir, Freundlich, Temkin, and D-R), and thermodynamics parameters (ΔG^o, ΔH^o, *and* ΔS^o) were also carried out to identify the adsorption properties of the adsorbent. Ag_2O nanoparticles were regenerated and reused to remove SMX. The optimized geometries, highest occupied and lowest unoccupied molecular orbitals (HOMO-LUMO), and electrostatic potential (ESP) maps corresponding to the and quantum chemical parameters (E_{HOMO}, $E_{HOMO,}$ $\Delta E_{gap,}$ μ, χ, η, and σ) of the SMX unprotonated ($SMX^{+/-}$) and protonated (SMX^+) were investigated using calculations based on DFT/B3LYP 6–31 + G (d,p) under the solvation conditions. Finally, a possible mechanism of SMX adsorption on Ag_2O NPs was proposed.

2 Methodology

2.1 Chemicals and instrumentations

Hydrochloric acid (HCl), acetone, methanol, sodium hydroxide (NaOH), potassium nitrate (KNO_3), ethanol, and SMX antibiotic have been purchased from Sigma-Aldrich and have analytical quality. Distilled water was used in all experiments. The characteristics of SMX are summarized in Table 1.

Table 1. Physicochemical characteristics of SMX.

Characteristic	Value
Class	Sulfonamid antibiotic
IUPAC name	4-amino-N-(5-methyl-1,2-oxazol-3-yl)benzenesulfonamide
Moleular structure	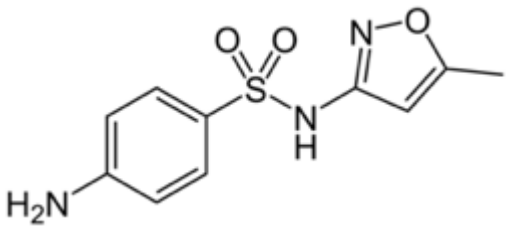
Formula	$C_{10}H_{11}N_3O_3S$
λ_{max} (nm)	263
Molecular weight (g mol^{-1})	253.279
pka1	1.97
pka_2	6.16
Polarisability	24.16
Diffusion coefficient (10^{-1} m^2 s^{-1}) [2]	6.25

The surface properties of GP-C and GPAC

Experiments of X-ray diffraction (XRD) are performed on a Bruker D8 Advance Twin diffractometer to determine the nature of the crystals of Ag_2O nanoparticles. The FTIR spectrum of Ag_2O NPs has been obtained using ATR technique on IR JASCO 4100 spectrophotometer and scanned on a wavelength range from 500 to 4000 cm^{-1}. The surface properties of Ag_2O NPs were determined by Brunauer-Emmett-Teller analysis (BET, Belsorp Mini II). The morphology characteristics of Ag_2O NPs was identified using Scanning Electron microscopy with energy dispersive X-ray analysis (SEM-EDX, JEOL, JSMIT200) and transmission electron microscope (TEM, JEOL Ltd, Tokyo, Japan). The point of zero charge (PZC) of Ag_2O NPs has been determined according to the process reported by El Messaoudi et al. (El Messaoudi et al. 2022b).

2.2 Green synthesis of Ag_2O NPs

The *Punica granatum* leaves (PGL) were obtained from an area of Tinghir (Morocco). The PGL were cleaned thoroughly using distilled water to eliminate dirt, dust, and other surface contaminants before sun drying. The cleaned PGL then were soaked in methanol for 24 h to remove the pigments and fat, and then washed with distilled water several times dried in the dryer for 12 h. The dry biomaterial was ground by a mechanical grinder and screened at 50 µm. 10 g PGL powder was added to 50 mL of distilled water for 2 h at 70°C. After that, the mixture was filtered and centrifuged to separate the water extract and the residue of the PGL powder. 20 mL of the obtained extract was added to 40 mL of a solution consisting of $AgNO_3$ (0.2 M) and 5 mL of NaOH (0.1 M), stirring continuously for 5 h at 65°C. After precipitation, the sample was rinsed with distilled water multiple times and then dried in 16 the dryer for 12 h at 70°C, and then calcined in an oven at 450°C for 3 h. The green synthesis process of Ag_2O nanoparticles from *Punica granatum* leaf extract is detailed in Fig. 1.

2.3 Adsorption experiments

The batch adsorption experiments were performed in an aqueous solution. The adsorption performance of Ag_2O NPs was evaluated for the removal of SMX to identify the effect of operating conditions, including adsorbent dosage (0.2–1.4 g L^{-1}), initial SMX concentration (50–400 mg L^{-1}), initial pH of antibiotic solution (2–10) and contact time (5–180 min) at temperature (298–318 K). Evaluation of adsorption capacity was analyzed using the isotherm studies carried out at 298 K, 308 K, and 318 K by equilibrating Ag_2O NPs (40 mg) with 50 mL of SMX solution (50–400 mg L^{-1}) for 90 min at solution pH = 4, while kinetics and thermodynamic experiments were conducted in a similar way at three different initial SMX concentrations 100 mg L^{-1}, 150 mg L^{-1}, and 200 mg L^{-1} for 5–180 min, and at the above three temperatures, respectively. After each adsorption experiment, the antibiotic solution was filtered using a syringe filter (0.45 µm), and the concentration of the final solution was determined using a UV-visible spectrophotometer (UV/Vis 2300) at a maximum absorbance wavelength of 263 nm. The removal percentage (%) of the SMX solution was determined using Eq. (1):

$$\%Removal = \frac{\left(C_i - C_f\right)}{C_i} \times 100 (1)$$

C_i (mg L^{-1}) and C_f (mg L^{-1}) refer to the initial and final concentrations of SMX, respectively.

The amount of SMX adsorption at equilibrium, q_e (mg L^{-1}) was determined from Eq. (2):

$$q_e = \frac{\left(C_i - C_f\right) \times V}{m} (2)$$

V/m (g L^{-1}) denotes the adsorbent dosage.

2.4 DFT computational

The electronic structure calculations were performed with Gaussian 9 software packages. The equilibrium structure of the unprotonoted ($SMX^{+/-}$) and protonoted (SMX^{+}), as well the parameters, E_{HOMO}, E_{LUMO}, energy gap (ΔE_{gap}), ESP maps, dipole moment (μ), and parameters that give valuable information on the reactive behavior such as the electronegativity (χ) ionization, hardness (η), softness (σ) were determined using density functional theory (DFT) combined with the Lee-Yang-Parr correlation function (B3LYP) (Becke 1993; Stephens et al. 1994) and the 6–31 + G (d,p) basis set (Kendall et al. 1992). All calculations were performed in the aqueous phase. The quantum parameters are presented by mathematical formulas as follows:

$$\Delta E_{gap} = E_{LUMO} - E_{HOMO} \quad (3)$$

$$\chi = \frac{-\left(E_{LUMO} + E_{HOMO}\right)}{2} \quad (4)$$

$$\eta = \frac{\left(E_{LUMO} - E_{HOMO}\right)}{2} \quad (5)$$

$$\sigma = \frac{1}{n} \quad (6)$$

3 Results And Discussion

3.1 Ag_2O NPs characterization

XRD is one of the most widely used methods for characterizing the structure of an Ag_2O nanoparticle. XRD graph gives the most direct results such as crystallinity. The XRD results obtained (Fig. 2a) show almost identical plots and exhibit the same intense diffraction peaks at 38.6°, 45°, 65°, 75.4°, and 81.6° with (111), (200), (220), (311), and (222) planes (JCPDS 00-041-1106), respectively that are attributed to Ag_2O (Bian et al. 2020). From Fig. 2a, it is clear that the crystallinity of Ag_2O NPs and maintained at a face-centered cubic crystal structure (Rashmi et al. 2020; Zamanpour et al. 2021).

Figure 2b exhibits the infrared spectrum of Ag_2O NPs. The analysis was performed over a range of wavelengths from 500 to 4000 cm^{-1}. The peaks at 3407 cm^{-1} and 1623 cm^{-1} may arise due to O—H stretching mode of absorbed water molecules (Xu et al. 2013b). The bonds observed around 546 cm^{-1} and 718 cm^{-1} are corresponds to the stretching vibration of the Ag-O group (Ananth and Mok 2016; Bhogal et al. 2020).

The surface properties of Ag_2O NPs were identified by using BET analysis (Fig. 2c). The BET surface area of Ag_2O NPs was found to be 107.09 $m^2\ g^{-1}$, and the result obtained revealed that Ag_2O NPs has a

higher porosity with a total pore volume and average pore diameter was 0.38 m^3 g^{-1}, and 31 nm, respectively.

The morphology of the adsorbent was analyzed by using SEM analysis. Figure 3a shows the micrograph of Ag_2O NPs. The spherical shapes of the particles are clearly evident from the SEM image, and irregular structure with pores of different shapes and sizes, provide enough surface area for interaction with SMX molecules (Xu et al. 2013a; Abdalameer et al. 2021). The EDX spectra (Fig. 3b) showed the major elements detected as O (25.80%), and Ag (74.20%) similar to that reported by Mohammadi et al. (Mohammadi et al. 2019) and Haq et al. (Haq et al. 2018).

The TEM image of Ag_2O NPs obtained, as shown in Fig. 3c. This image presents the highly ordered porous structure of Ag_2O NPs, and spherical in the shape of the particles (Ahmad and Majid 2018). The bioactive compounds trapped on the surface of Ag_2O NPs can be attributed to the Ag_2O NPs surrounding the thin layer (Camacho-Escobar et al. 2020). The size and average of nanoparticles ranged from 24 to 36 nm confirming that the Ag_2O NPs synthesized were in the nano-scale range.

3.2 Adsorption studies

3.2.1 Effect of solution pH

Figure 4a displays the SMX speciation diagram as a function of the solution pH. The SMX displays a pKa couple of 1.97 (pKa_1) and 6.16 (pKa_2), between these values the SMX has the unprotonated form ($SMX^{+/-}$), while charged positively (SMX^+) at pH < pKa_1 and negatively (SMX^-) at pH > pKa_2 (De Oliveira et al. 2018). The effect of pH on SMX adsorption onto Ag_2O NPs was investigated at different pH values ranging from 2 to 10 (Fig. 4b) at the kept factorial values (time = 180 min, temperature = 298 K, concentration = 100 mg L^{-1}, and Ag_2O NPs dose = 1 g L^{-1}). Acidic pH promotes protonation of the Ag-O group ($Ag\text{-}OH_2^+$) resulting in acidic adsorption sites. Excess of H^+ ions battle against the positive groups of antibiotic (SMX^+) for adsorption surface, resulting in repulsion among the Ag-O group ($Ag\text{-}OH_2^+$) of adsorbent and SMX^+ and antibiotic adsorption is disfavored. Whereas basic pH causes deprotonating of Ag-O group ($Ag\text{-}O^-$) of adsorbent, more hydroxide ions render adsorption of SMX^-, making the surface negatively charged of Ag_2O NPS and antibiotic adsorption is also disfavored. The pH range 2–10 was selected for the sequestration of the SMX antibiotic. SMX adsorption depends upon charge and surface characteristics. The PZC of Ag_2O NPs was found to be 5.3. At pH < PZC, the adsorbent is positively charged ($Ag\text{-}OH_2^+$) while it is negative at pH > PZC (Taher et al. 2021), the repulsive forces resulting between the $Ag\text{-}OH_2^+$ and $Ag\text{-}O^-$ groups and SMX^+ and SMX^-, respectively, therefore, the SMX adsorption is unfavorable. At pH near PZC (zwitterionic), the attractive forces result between the $Ag\text{-}OH_2^+$ and $Ag\text{-}O^-$ groups of adsorbent and $SMX^{+/-}$ antibiotic, thus antibiotic adsorption is favored. The result obtained is similar to that reported by Zhang et al. (2010) (Zhang et al. 2010). The highest uptake quantity of SMX was 122.45 mg g^{-1} at pH = 4.

3.2.2 Effect of adsorbent dose

The effect of Ag_2O dosage on the SMX adsorption was examined in the range 0.2–1.4 g L^{-1} (Fig. 4c), while the other conditions are kept at the central value (time = 180 min, temperature = 298 K, concentration = 100 mg L^{-1}, and pH = 4). The SMX removal increased from 60.29 to 98.19% by increasing the adsorbent dose from 0.2 to 0.8 g L^{-1} because large nanoparticle production provides an outspread surface area of the adsorbent which provides numerous active adsorbent sites for the antibiotic to get adsorbed. Hence more active site accessibility for the SMX molecules to adsorb (El Messaoudi et al. 2022a). After reaching maximum adsorption efficiency (> 0.8 g L^{-1}), an increase in dosage does not have much antibiotic sequestration efficiency. This is due to the gradient distribution between the Ag_2O NPs and antibiotic as well as active sites saturation (Ogunleye et al. 2020). Adsorption capacity decreased (301.49 – 70.46 mg g^{-1}) with adsorbent dose from 0.2 to 1.4 g L^{-1} due to an increase in unsaturated sites with an increase in the adsorbent dose and a rise in SMX concentrations (Ahsan et al. 2018). Hence, 0.8 g L^{-1} of the adsorbent dose was selected for further experiments as higher concentrations did not yield significant results.

3.2.3 Effect of contact time

SMX antibiotic sequestration by Ag_2O NPs is determined by finding the least time required for achieving equilibrium of antibiotic with the adsorbent in the range 5–180 min for three concentrations (100, 150, and 200 mg L^{-1}) at experiment conditions (Ag_2O NPs dose = 0.8 g L^{-1}, T = 298 K, and pH = 4) (Fig. 5a). Noting strong adsorption of the SMX on the Ag_2O NPs from the first minutes of contact between the antibiotic and the adsorbent is due to the number of active sites available on the surface (Guo et al. 2019). The balance of adsorption is reached in 90 min, beyond this time, it was found that the amount adsorbed for 100 mg L^{-1} is about 122.78 mg g^{-1}, 181.61 mg g^{-1} for 150 mg L^{-1}, and 231.12 mg g^{-1} for 200 mg L^{-1}. After 90 min, the SMX adsorption capacity became de-escalate due to the occupation of active sites of Ag_2O NPs (Liu et al. 2017). Therefore, 90 min is considered the equilibrium time optimum.

3.2.4 Effect of SMX concentration and temperature

The influence of initial SMS concentration at three temperatures 298 K, 308 K, and 318 K on SMX adsorption using Ag_2O NPs is shown in Fig. 5b. To investigate the effect of initial antibiotic concentration on SMX adsorption, the antibiotic concentration was varied from 50 to 400 mg L^{-1}. It is noted that the adsorption capacity of SMX increased from 60.96 to 250.26 mg g^{-1} for 298K, from 61.57 to 260.14 mg g^{-1} for 308 K, and from 61.98 to 276.48 mg g^{-1} for 318 K with SMX concentration from 50 to 250 mg L^{-1}. This is because at a low concentration range the ratio between the Ag_2O NPs surface and the SMX molecules in the solution are in abundance, therefore all of the antibiotic particles are easily imbibed over the surface of the active adsorbed and get eliminated from the media (Guo et al. 2019). After 250 mg L^{-1} of SMX concentration, the adsorption capacity was achieved. This is because at higher concentrations the driving force is also higher due to the concentration gradient and the adsorbed amount of the

antibiotic per unit mass of the Ag_2O NPs is also high which leads to the saturation of active sites (Liu et al. 2017).

Figure 5b also shows the effect of temperature on the adsorption capacity of SMX. It is evident that q_e increases with temperature from 298 to 318 K, which may probably be due to the high rate of mass transfer from the bulk solution to a solid phase, widening of pore size, and/or activation of adsorption sites (Fulazzaky 2011). Additionally, an enhancement in the quantity adsorbed with temperature is descriptive of the endothermic nature of adsorption (El Messaoudi et al. 2021b), this is confirmed by thermodynamic and equilibrium isotherm studies subsequently.

3.3 Adsorption modeling

3.3.1 Kinetics

The dynamics of the adsorption of SMX onto Ag_2O NPs were investigated using Lagergren's

pseudo-1st -order model (PFO) (Lagergren 1898), pseudo-2nd -order (PSO) model proposed by Ho and McKay (Ho and McKay 1998) and intraparticle diffusion model (IPD) (El Messaoudi et al. 2022b). The K_{PFO} (PFO constant) was calculated from the plot of log (q_e-q_t) versus t (Fig. 6a), while the plot of t/q_t versus t (Fig. 6b), and gives the value of K_{PSO} (PSO constant), which are tabulated in Table 2 along with R^2 values. Comparatively lower R^2 values for PFO model along with the evident deviation from linearity suggest incongruity of the model with the kinetic data thus ruling out the possibility of interaction of the antibiotic molecule with a single active site. However, the linearity of the t/q_t versus t plots and high R^2 values (0.999) reflects that adsorption conforms better to the PSO kinetic model. Moreover, calculated equilibrium capacities $q_{e,PSO}$ are in complete agreement with that of experimental equilibrium capacities $q_{e,exp}$. It is, therefore, concluded that the rate of adsorption of SMX onto Ag_2O NPs for three concentrations (100, 150, and 200 mg L^{-1}) is related to the square of the number of available active sites and a single antibiotic molecule is capable of interacting with two adsorption sites simultaneously (Wang et al. 2015). This is similar to reports on the adsorption of SMX onto the Fe-impregnated graphited biochar (Zhang et al. 2020) and montmorillonite (Wu et al. 2019) adsorbents.

Table 2
Kinetic models constants for SMX adsorption on Ag_2O NPs.

Model		Parameter	SMX conc. (mg L^{-1})		
			100	150	200
		$q_{e,exp}$ (mg g^{-1})	123.87	182.23	233.87
PFO $Log(q_e - q_t) = Log(q_e) - \frac{K_{PFO}}{2.303}t$		$q_{e,PFO}$ (mg g^{-1})	39.79	92.44	147.40
		K_{PFO} (min^{-1})	0.030	0.033	0.035
		R^2	0.926	0.923	0.954
PSO $\frac{t}{q_t} = \frac{1}{K_{PSO}{q_e}^2} + \frac{1}{q_e}t$		$q_{e,PSO}$ (mg g^{-1})	126.58	192.30	238.09
		K_{PSO} (g mg^{-1} min^{-1})	0.0017	0.0019	0.0024
		R^2	0.999	0.998	0.998
IPD $q_t = K_{IDP}t^{1/2} + C_i$	1st linear portion	K_{IPD1} (mg g^{-1} $min^{-1/2}$)	14.303	16.215	21.198
		C_1 (mg g^{-1})	41.31	58.04	60.42
		R^2	0.958	0.978	0.975
	2nd linear portion	K_{IPD2} (mg g^{-1} $min^{-1/2}$)	4.523	10.149	12.745
		C_2 (mg g^{-1})	83.28	78.22	115.06
		R^2	0.997	0.996	0.966
	3th linear portion	K_{IPD3} (mg g^{-1} $min^{-1/2}$)	0.237	0.368	0.641
		C_3 (mg g^{-1})	120.39	177.92	225.06
		R^2	0.859	0.873	0.961

The intraparticle diffusion model controls the process when the three basic adsorption steps, that is, instant, gradual and equilibrium adsorptions become indistinguishable (El Messaoudi et al. 2022b). The slope and intercept of q_t versus $t^{1/2}$ plots give the values of K_{IPD} (IPD constant) and C_i (boundary layer thickness) at three different concentrations (Fig. 6c), which are tabulated in Table 2. From Fig. 6c, the SMX adsorption process on Ag_2O NPs presents in three successive stages. The first stage describes the diffusion of SMX molecules from the aqueous phase to the external surface sites of Ag_2O NPs (Ahmed et

al. 2021). The second phase indicates the intraparticle diffusion of SMX species into the internal surface of Ag_2O NPs with a rate-controlling step (Tavlieva et al. 2013). The values of C_2 (83.28–115.06 mg g^{-1}) illustrate that liquid film diffusion plays a dominant contribution to the overall rate-controlling step for three concentrations (100, 150, and 200 mg L^{-1}). The third step corresponds to adsorption equilibrium because of the extremely low concentration of SMX (Yao and Chen 2017).

3.3.2 Equilibrium

To understand the mechanisms involved in the adsorption of SMX on Ag_2O NPs at three temperatures (298, 308, and 318 K), four isotherm models are use such as Langmuir, Freundlich, Temkin, and Dubinin–Radushkevich (D-R). The Langmuir model is very useful for the monomolecular adsorption of a solute by forming a monolayer on the surface of the adsorbent (Langmuir 1918). The Freundlich model is based on adsorption on heterogeneous surfaces (Freundlich 1907). Temkin isotherm model contemplates a linear decline in the heat of adsorption of molecules in the layer with surface coverage as an indirect consequence of adsorbate-adsorbent interactions, and the homogeneous distribution of binding energies characterizes the adsorption process (Johnson and Arnold 1995). Dubinin–Radushkevich (D-R) isotherm is associated with multilayer adsorption with a tendency of adsorbate molecules to fill the micropores (Çelebi et al. 2007; Ayawei et al. 2017). It is also generally utilized for the prediction of the adsorption mechanism (Chen and Yang 2002; Gallego-Gómez et al. 2020).

The values of Q_m (maximum adsorption capacity) and K_L (Langmuir constant) at three different temperatures (298–318 K) were obtained from the slope and intercept, respectively of C_e/q_e versus C_e plots (Fig. 7a). The values of K_F (Freundlich constant) and $1/n_F$ (heterogeneity factor) were obtained from the slope and intercept respectively of the linear $\ln q_e$ versus $\ln C_e$ plots (Fig. 7b). A linear plot of q_e versus $\ln C_e$ (Fig. 7c) gives the values of Temkin constants, K_T (Temkin constant) and b_T from its slope and intercept, respectively. The linear curves of $\ln q_e$ versus ε^2 (D-R constant, $\varepsilon = RT\ln(1 + 1/Ce)$) (Fig. 7d) were used to determine the Q_m and β from the slope and intercept, respectively. From Table 3, the values of K_L, which denotes the binding affinity or strength of antibiotic molecules with Ag_2O NPs surface show a gradual increment from 0.232 to 0.394 L mg^{-1} with raise in solution temperature (298 to 318 K) indicating thereby an improved SMX-Ag_2O NPs binding strength at elevated temperature. The higher *Qm*, which is often considered a measure of the efficacy of an adsorbent (277.85–312.59 mg g^{-1}) confirms the efficient adsorption performance of Ag_2O NPs at all tested temperatures. An ascending trend in K_F from 82.121 to 109.039 mg g^{-1} with rising in operating temperature from 298 to 318 K is illustrative of the endothermic adsorption of SMX. The calculated values of $1/n_F$ (0.248–0.259) are positive but less than one which advocates favorable adsorption in the studied temperature range. The correlation coefficient R^2 values for the Langmuir model is higher (0.999) for three temperatures signifying a good fit of the equilibrium data at high temperatures. The constant K_T increases from 6.903 to 16.014 L mg^{-1} with temperature further confirms the endothermic nature of SMX adsorption. The adsorption energy value ($E = 1/(2\ \beta)^{1/2}$) is functional in describing the nature of the adsorption mechanism ($E < 8$ kJ mol^{-1}

physisorption; E > 16 kJ mol^{-1} chemisorption; and 8 ≤ E ≤ 16 kJ/ mol^{-1}: ion exchange) (Isiuku et al. 2021). The E values in the 0.845–2.236 kJ mol^{-1} range reflect the physical mode of the adsorption. The R^2 values for the Langmuir model (0.999) are considerably close to unity relative to Freundlich (0.847–0.868), Temkin (0.942–0.957), and D–R (0.817–0.898) models, which describes that the equilibrium data is more appropriately explicated by the Langmuir model, suggesting that monolayer adsorption of SMX on Ag_2O NPs (Wu et al. 2019). The performance appraisal of Ag_2O NPs based on comparative *Qm* values of hitherto reported adsorbents for SMX removal (Table 4), reveals that the present adsorbent has shown superior uptake competence outperforming the existing adsorbents.

Table 3
Isotherm models constants for SMX adsorption on Ag_2O NPs.

Model	Parameter	Temperature (K)		
		298	**308**	**318**
Langmuir $\frac{C_e}{q_e} = + \frac{C_e}{Q_m} + \frac{C_e}{Q_m}$	Q_m (mg g^{-1})	277.85	295.85	312.59
	K_L (L mg^{-1})	0.232	0.262	0.394
	R^2	0.999	0.999	0.999
Freundlich $Lnq_e = LnK_F + \frac{LnC_e}{n_F}$	K_F (mg g^{-1})	82.121	92.489	109.039
	$1/n_F$	0.259	0.252	0.248
	R^2	0.847	0.870	0.868
Temkin $q_e = \frac{RT}{b_T} LnK_T + \frac{RT}{b_T} LnC_e$	b_T (kJ mol^{-1})	0.061	0.064	0.072
	K_T (L mg^{-1})	6.903	9.130	16.014
	R^2	0.942	0.959	0.957
D-R $Lnq_e = LnQ_m - \beta\epsilon^2$	Q_m (mg g^{-1})	232.64	242.79	250.46
	E (kJ mol^{-1})	0.845	1.290	2.236
	R^2	0.898	0.851	0.817

Table 4
Q_m of Ag_2O NPs for SMX removal compared with other adsorbents.

Adsorbent	Q_m (mg g^{-1})	Reference
Fe-impregnated graphited biochar	205.00	(Zhang et al. 2020)
carbonnanotubes/$CoFe_2O_4$	248.91	(Wang et al. 2015)
$CuZnFe_2O_4$/biochar	213.00	(Heo et al. 2019)
Magnetic activated carbon	173.00	(Lv et al. 2021)
Activated carbon	113.00	(Jaria et al. 2021)
AC functionalized with thiol groups	140.00	(Jaria et al. 2021)
Fe_3O_4 /pectin-waste biomass	120.00	(Kadam et al. 2020)
Tea waste-SO_3H	258.87	(Ahsan et al. 2018)
Commercially available activated carbon	118.00	(Calisto et al. 2015)
Graphene oxide	240.00	(Chen et al. 2015)
Ag_2O NPs	277.85	Current study

3.4 Thermodynamic studies

The study of the thermodynamics of the adsorption process is useful in obtaining the information related to the feasibility/spontaneity, exothermic/endothermic and disorder at the solid-solution interface based on the evaluated values of changes in Gibbs free energy (ΔG^o), enthalpy change (ΔH^o) and entropy (ΔS^o) change, respectively. The values of ΔH^o and ΔS^o were obtained from the slope and intercept of the linear plot of $\ln K_d$ versus $1/T$ (Fig. 8a) according to Eq. 8, while ΔG^o was computed using Eq. 7 (El Messaoudi et al. 2021c):

$$\Delta G^\circ = -RTLnK_d (7)$$

$$LnK_d = \frac{\Delta S^\circ}{R} - \frac{\Delta H^\circ}{RT} (8)$$

where, R (8.314 J mol^{-1} K^{-1}) is the universal gas constant and T (K) is the absolute temperature, and K_d is the distribution coefficient defined as q_e/C_e. The values of the thermodynamic parameters are given in Table 5. For the SMX adsorption onto the Ag_2O NPs, the negative ΔG^o at all studied temperatures infers the feasibility of the process for three concentrations (100, 150, and 200 mg L^{-1}). Further, the increase of ΔG^o with temperature shows that SMX removal is spontaneous and more promising at higher temperatures (Ahmed et al. 2021). This is supported by the positive ΔH^o, which affirms the endothermic

adsorption (Serna-Carrizales et al. 2021). Entropy change is a measure of the change in randomness at the solid-liquid interface. The positive ΔS^o values (108.523–132.484 J mol^{-1} K^{-1}) indicate the increase in randomness of SMX adsorption (Fierro et al. 2007).

Table 5
Thermodynamic parameters for the SMX adsorption toward Ag_2O NPs.

SMX conc. (mg L^{-1})	T (K)	$\Delta G°$ (kJ mol^{-1})	$\Delta H°$ (kJ mol^{-1})	$\Delta S°$ (J mol^{-1} K^{-1})
100	298	−08 .741	23.619	108.523
	308	−09.798		
	318	−10.925		
150	298	−06.917	27.712	114.461
	308	−08.117		
	318	−09.927		
200	298	−05.584	33.887	132.484
	308	−06.942		
	318	−08.241		

3.5 Recyclability of Ag_2O NPs

The reusability experiment gives useful insights into the possibility of recovery and operational behavior of the adsorbent. The recyclability of Ag_2O NPs for the removal of SMX was tested after acetone and ethanol washing. The results are summarized in Fig. 8b. The difference in percentage removal between the first and five uses of Ag_2O NPs adsorbent for removal of SMX was 22% at optimal conditions: 0.8 g L^{-1} of adsorbent dose, pH of 4, 100 mg L^{-1} of SMX concentration at 308 ± 1 K for 90 min. Still, further research is required for the usage of Ag_2O NPs for antibiotics removal from wastewaters.

3.6 DFT results

The analysis of the HOMO and LUMO energy levels, as well as the gap energy, is very important in the study of the properties of organic molecules (Jodeh et al. 2022). The energies of the HOMO and LUMO frontier orbitals and the gap energy of the molecules calculated by the DFT/B3LYP 6–31 + G (d,p) method under different pH conditions from the optimized structures are given in Table 6, a unprotonated and protonated state. From this table, we notice that the SMX^+ molecule has the highest energy gap ΔE_{gap}=5.717 eV, therefore it is the most stable and the least chemically active (Zhuang et al. 2020). In the case of $SMX^{+/-}$, it has the lowest energy gap ΔE_{gap}=5.197 eV, so it is the least stable and the most chemically active (Liu et al. 2020b). The importance of η and σ is to evaluate both reactivity and stability. The neutral form of SMX has the lowest value of chemical hardness (η = 2.598 eV), which means high

reactivity compared to the protonated form (Alivand et al. 2019). Global reactivity plays an important role to describe the ability of SMX to interact with the surface of Ag_2O NPs under different pH conditions. Optimized geometries, HOMO, LUMO frontier orbitals, and ESP maps corresponding to the two forms of SMX are presented in Fig. 9. This figure shows that the backbone of the SMX molecule in both the proton and unproton forms is characterized by positive potential (i.e. the blue regions in Fig. 9d and **g**) (Obot and Obi-Egbedi 2010). According to these observations, the non-protonated molecule is reacting more favorably on the surface of Ag_2O NPs. These results are in good agreement with those obtained experimentally.

Table 6
Quantum chemical parameters for the SMX unprotonated and protonated.

SMX	E_{HOMO} (eV)	E_{LUMO} (eV)	ΔE_{gap} (eV)	η (eV)	χ (eV)	σ (eV^{-1})	μ(D)
$SMX^{+/-}$	−6.278	−1.081	5.197	2.598	3.680	0.386	15.55
SMX^{+}	−8.359	−2.642	5.717	2.858	5.500	0.349	11.761
Graphical abstract							

3.7 Proposed adsorption mechanism

The FTIR and PZC of Ag_2O NPs, DFT calculation of SMX, and the influence of operational solution pH are mainly functional in understanding the type of interactions taking place between the surface of Ag_2O NPs and SMX molecules. Since q_e was relatively unaltered with change in the initial pH, the possibility of interactions is excluded, thus pointing towards the involvement of hydrogen-bonding, hydrophobic, and π-π interactions (Fig. 10) (Eniola et al. 2019; Ahmed et al. 2021). The interactions were of the physical kind, which is supported by the D-R isotherm model study which established the physical nature of adsorption.

4 Conclusions

Ag_2O nanoparticle has been successfully prepared by the green synthesis method from *Punica granatum* leaf extract. The XRD, FTIR, BET, SEM-EDX, TEM, and PZC techniques were used to examine the structural, morphological, and chemical properties of the Ag_2O NPs. At optimal operating conditions (time = 90 min, Ag_2O NPs dose = 0.8 g L^{-1}, SMX concentration = 100 mg L^{-1}, T = 308 K, and pH = 4), the removal and adsorption capacity of SMX were 98.93% and 122.63 mg g^{-1}, respectively. The kinetics of SMX adsorption was best appropriated by the PSO model. The adsorption was best explained by the Langmuir isotherm model, thus defining monolayer SMX adsorption onto homogeneous Ag_2O NPs surface. Thermodynamically, the adsorption process revealed an endothermic nature and confirmed the feasibility and spontaneity of the reaction. Langmuir adsorption capacity of 277.85 mg g^{-1} was considerably higher than those reported previously. The experimental results are in good agreement with those obtained by DFT calculation. Hydrogen-bonding, hydrophobic, and π-π interactions were majorly involved in the SMX uptake by Ag_2O NPs.

Declarations

Data availability

The datasets used during the current study are available from the corresponding author on reasonable request.

Author Contributions

Noureddine El Messaoudi: Investigation and Writing-original draft; **Abdelaziz El Mouden**: Verification and Methodology; **Yasmine Fernine**: Software and Review editing; **Mohammed El Khomri**: Verification, Validation, and Methodology; **Amal Bouich**: Verification, Validation, and Methodology; **Nadia Faska**: Review editing; **Zeynep Ciğeroğlu**: Review editing, Conceptualization, and Visualization; **Juliana Heloisa Pinê Américo-Pinheiro**: Review editing; **Amane Jada**: Review editing, and Conceptualization; **Abdellah Lacherai**: Review editing, Conceptualization, and Supervision.

Compliance with ethical standards

Ethics approval and consent to participate

Not applicable.

Funding

No funding.

Consent for publication

Not applicable.

Competing interests

The authors declare that they have no competing interests.

References

1. Abdalameer NK, Khalaph KA, Ali EM (2021) Ag/AgO nanoparticles: Green synthesis and investigation of their bacterial inhibition effects. Mater Today Proc 45:5788–5792. https://doi.org/10.1016/J.MATPR.2021.03.166
2. Ahmad J, Majid K (2018) In-situ synthesis of visible-light responsive Ag2O/graphene oxide nanocomposites and effect of graphene oxide content on its photocatalytic activity. Adv Compos Hybrid Mater 2018 12 1:374–388. https://doi.org/10.1007/S42114-018-0025-6
3. Ahmed I, Adhikary KK, Kim K, Ahn WS (2021) Aqueous adsorption of sulfamethoxazole on an N-doped zeolite beta-templated carbon. J Colloid Interface Sci 582:467–477.

https://doi.org/10.1016/J.JCIS.2020.08.065

4. Ahsan MA, Islam MT, Hernandez C et al (2018) Adsorptive Removal of Sulfamethoxazole and Bisphenol A from Contaminated Water using Functionalized Carbonaceous Material Derived from Tea Leaves. J Environ Chem Eng 6:4215–4225. https://doi.org/10.1016/J.JECE.2018.06.022
5. Alivand MS, Najmi M, Tehrani NHMH et al (2019) Tuning the surface chemistry and porosity of waste-derived nanoporous materials toward exceptional performance in antibiotic adsorption: Experimental and DFT studies. Chem Eng J 374:274–291. https://doi.org/10.1016/J.CEJ.2019.05.188
6. Ananth A, Mok YS (2016) Dielectric Barrier Discharge (DBD) Plasma Assisted Synthesis of Ag2O Nanomaterials and Ag2O/RuO2 Nanocomposites. Nanomater 2016, Vol 6, Page 42 6:42. https://doi.org/10.3390/NANO6030042
7. Asghar MA, Zahir E, Shahid SM et al (2018) Iron, copper and silver nanoparticles: Green synthesis using green and black tea leaves extracts and evaluation of antibacterial, antifungal and aflatoxin B1 adsorption activity. LWT 90:98–107. https://doi.org/10.1016/J.LWT.2017.12.009
8. Ayawei N, Ebelegi AN, Wankasi D (2017) Modelling and Interpretation of Adsorption Isotherms. J Chem 2017. https://doi.org/10.1155/2017/3039817
9. Becke AD (1993) Density-functional thermochemistry. III. The role of exact exchange. J Chem Phys 98:5648. https://doi.org/10.1063/1.464913
10. Berges J, Moles S, Ormad MP et al (2021) Antibiotics removal from aquatic environments: adsorption of enrofloxacin, trimethoprim, sulfadiazine, and amoxicillin on vegetal powdered activated carbon. Environ Sci Pollut Res 28:8442–8452. https://doi.org/10.1007/S11356-020-10972-0/FIGURES/6
11. Bhogal S, Sharma G, Kumar A et al (2020) Ag2O–Al2O3–ZrO2 Trimetallic Nanocatalyst for High Performance Photodegradation of Nicosulfuron Herbicide. Top Catal 2020 6311 63:1272–1285. https://doi.org/10.1007/S11244-020-01381-1
12. Bian H, Zhang Z, Xu X et al (2020) Photocatalytic activity of Ag/ZnO /AgO/TiO2 composite. Phys E Low-dimensional Syst Nanostructures 124:114236. https://doi.org/10.1016/J.PHYSE.2020.114236
13. Braschi I, Martucci A, Blasioli S et al (2016) Effect of humic monomers on the adsorption of sulfamethoxazole sulfonamide antibiotic into a high silica zeolite Y: An interdisciplinary study. Chemosphere 155:444–452. https://doi.org/10.1016/J.CHEMOSPHERE.2016.04.008
14. Calisto V, Ferreira CIA, Oliveira JABP et al (2015) Adsorptive removal of pharmaceuticals from water by commercial and waste-based carbons. J Environ Manage 152:83–90. https://doi.org/10.1016/J.JENVMAN.2015.01.019
15. Camacho-Escobar L, Palma-Goyes RE, Ortiz-Landeros J et al (2020) Unraveling the structural and composition properties associated with the enhancement of the photocatalytic activity under visible light of Ag2O/BiFeO3-Ag synthesized by microwave-assisted hydrothermal method. Appl Surf Sci 521:146357. https://doi.org/10.1016/J.APSUSC.2020.146357

16. Çelebi O, Üzüm Ç, Shahwan T, Erten HN (2007) A radiotracer study of the adsorption behavior of aqueous Ba2 + ions on nanoparticles of zero-valent iron. J Hazard Mater 148:761–767. https://doi.org/10.1016/J.JHAZMAT.2007.06.122
17. Chen H, Gao B, Li H (2015) Removal of sulfamethoxazole and ciprofloxacin from aqueous solutions by graphene oxide. J Hazard Mater 282:201–207. https://doi.org/10.1016/J.JHAZMAT.2014.03.063
18. Chen KL, Liu LC, Chen WR (2017) Adsorption of sulfamethoxazole and sulfapyridine antibiotics in high organic content soils. Environ Pollut 231:1163–1171. https://doi.org/10.1016/J.ENVPOL.2017.08.011
19. Chen SG, Yang RT (2002) Theoretical Basis for the Potential Theory Adsorption Isotherms. The Dubinin-Radushkevich and Dubinin-Astakhov Equations. Langmuir 10:4244–4249. https://doi.org/10.1021/LA00023A054
20. Cheong MS, Seo KH, Chohra H et al (2020) Influence of Sulfonamide Contamination Derived from Veterinary Antibiotics on Plant Growth and Development. Antibiot 2020, Vol 9, Page 456 9:456. https://doi.org/10.3390/ANTIBIOTICS9080456
21. De Oliveira T, Fernandez E, Fougère L et al (2018) Correction to “Competitive Association of Antibiotics with a Clay Mineral and Organoclay Derivatives as a Control of Their Lifetimes in the Environment”. ACS Omega 3:18433. https://doi.org/10.1021/ACSOMEGA.8B03327
22. Ehrampoush MH, Miria M, Salmani MH, Mahvi AH (2015) Cadmium removal from aqueous solution by green synthesis iron oxide nanoparticles with tangerine peel extract. J Environ Heal Sci Eng 13:1–7. https://doi.org/10.1186/S40201-015-0237-4/TABLES/2
23. El Khomri M, El Messaoudi N, Dbik A et al (2021) Removal of Congo red from aqueous solution in single and binary mixture systems using Argan nutshell wood. Pigment Resin Technol. https://doi.org/10.1108/PRT-04-2021-0045/FULL/XML
24. El Messaoudi N, El Khomri M, Ablouh EH et al (2022a) Biosynthesis of SiO2 nanoparticles using extract of Nerium oleander leaves for the removal of tetracycline antibiotic. Chemosphere 287:132453. https://doi.org/10.1016/J.CHEMOSPHERE.2021.132453
25. El Messaoudi N, El Khomri M, Chegini ZG et al (2021a) Desorption of crystal violet from alkali-treated agricultural material waste: an experimental study, kinetic, equilibrium and thermodynamic modeling. Pigment Resin Technol. https://doi.org/10.1108/PRT-02-2021-0019/FULL/XML
26. El Messaoudi N, El Khomri M, Chegini ZG et al (2021b) Dye removal from aqueous solution using nanocomposite synthesized from oxalic acid-modified agricultural solid waste and ZnFe2O4 nanoparticles. Nanotechnol Environ Eng 2021 71 7:1–15. https://doi.org/10.1007/S41204-021-00173-6
27. El Messaoudi N, El Khomri M, Dabagh A et al (2021c) Synthesis of a novel nanocomposite based on date stones/$CuFe_2O_4$ nanoparticles for eliminating cationic and anionic dyes from aqueous solution. Int J Environ Stud 1–19. https://doi.org/10.1080/00207233.2021.1929469
28. El Messaoudi N, El Khomri M, Fernine Y et al (2022b) Hydrothermally engineered Eriobotrya japonica leaves/MgO nanocomposites with potential applications in wastewater treatment. Groundw Sustain

Dev 16:100728. https://doi.org/10.1016/J.GSD.2022.100728

29. Eniola JO, Kumar R, Barakat MA (2019) Adsorptive removal of antibiotics from water over natural and modified adsorbents. Environ Sci Pollut Res 2019 2634 26:34775–34788. https://doi.org/10.1007/S11356-019-06641-6
30. Fair RJ, Tor Y (2014) Antibiotics and Bacterial Resistance in the 21st Century. Perspect Medicin Chem 6:25. https://doi.org/10.4137/PMC.S14459
31. Fierro V, Schuurman Y, Mirodatos C (2007) Simultaneous determination of intrinsic adsorption and diffusion of n-butane in activated carbons by using the TAP reactor. Stud Surf Sci Catal 160:241–247. https://doi.org/10.1016/S0167-2991(07)80032-2
32. Freundlich H (1907) Über die Adsorption in Lösungen. Z für Phys Chemie 57U:385–470. https://doi.org/10.1515/ZPCH-1907-5723
33. Fulazzaky MA (2011) Determining the resistance of mass transfer for adsorption of the surfactants onto granular activated carbons from hydrodynamic column. Chem Eng J 166:832–840. https://doi.org/10.1016/J.CEJ.2010.11.052
34. Gallego-Gómez F, Farrando-Pérez J, López C, Silvestre-Albero J (2020) Micropore Filling and Multilayer Formation in Stöber Spheres upon Water Adsorption. J Phys Chem C 124:20922–20930. https://doi.org/10.1021/ACS.JPCC.0C05313/SUPPL_FILE/JP0C05313_SI_001.PDF
35. Gao Y, Kang R, Xia J et al (2019) Understanding the adsorption of sulfonamide antibiotics on MIL-53s: Metal dependence of breathing effect and adsorptive performance in aqueous solution. J Colloid Interface Sci 535:159–168. https://doi.org/10.1016/J.JCIS.2018.09.090
36. Grenni P (2022) Antimicrobial Resistance in Rivers: A Review of the Genes Detected and New Challenges. Environ Toxicol Chem 41:687–714. https://doi.org/10.1002/ETC.5289
37. Guo S, Gao M, Shen T et al (2019) Effective adsorption of sulfamethoxazole by novel Organo-Vts and their mechanistic insights. Microporous Mesoporous Mater 286:36–44. https://doi.org/10.1016/J.MICROMESO.2019.05.032
38. Haq S, Rehman W, Waseem M et al (2018) Fabrication of pure and moxifloxacin functionalized silver oxide nanoparticles for photocatalytic and antimicrobial activity. J Photochem Photobiol B Biol 186:116–124. https://doi.org/10.1016/J.JPHOTOBIOL.2018.07.011
39. Heo J, Yoon Y, Lee G et al (2019) Enhanced adsorption of bisphenol A and sulfamethoxazole by a novel magnetic CuZnFe2O4–biochar composite. Bioresour Technol 281:179–187. https://doi.org/10.1016/J.BIORTECH.2019.02.091
40. Ho YS, McKay G (1998) Sorption of dye from aqueous solution by peat. Chem Eng J 70:115–124. https://doi.org/10.1016/S0923-0467(98)00076-1
41. Hwang IY, Koh E, Kim HR et al (2016) Reprogrammable microbial cell-based therapeutics against antibiotic-resistant bacteria. Drug Resist Updat 27:59–71. https://doi.org/10.1016/J.DRUP.2016.06.002
42. Isiuku BO, Enyoh CE, Duru CE, Ibe FC (2021) Phosphate ions removal from aqueous phase by batch adsorption on activated (activation before carbonization) biochar derived from rubber pod husk. Curr

Res Green Sustain Chem 4:100136. https://doi.org/10.1016/J.CRGSC.2021.100136

43. Jaria G, Calisto V, Gil MV et al (2021) Effects of thiol functionalization of a waste-derived activated carbon on the adsorption of sulfamethoxazole from water: Kinetic, equilibrium and thermodynamic studies. J Mol Liq 323:115003. https://doi.org/10.1016/J.MOLLIQ.2020.115003
44. Jodeh S, Jaber A, Hanbali G et al (2022) Experimental and theoretical study for removal of trimethoprim from wastewater using organically modified silica with pyrazole-3-carbaldehyde bridged to copper ions. BMC Chem 2022 161 16:1–17. https://doi.org/10.1186/S13065-022-00814-0
45. Johnson RD, Arnold FH (1995) The temkin isotherm describes heterogeneous protein adsorption. Biochim Biophys Acta - Protein Struct Mol Enzymol 1247:293–297. https://doi.org/10.1016/0167-4838(95)00006-G
46. Kadam AA, Sharma B, Saratale GD et al (2020) Super-magnetization of pectin from orange-peel biomass for sulfamethoxazole adsorption. Cellul 2020 276 27:3301–3318. https://doi.org/10.1007/S10570-020-02988-Z
47. Kendall RA, Dunning TH, Harrison RJ (1992) Electron affinities of the first-row atoms revisited. Systematic basis sets and wave functions. J Chem Phys 96:6796. https://doi.org/10.1063/1.462569
48. Khameneh B, Iranshahy M, Soheili V, Fazly Bazzaz BS (2019) Review on plant antimicrobials: a mechanistic viewpoint. Antimicrob Resist Infect Control 2019 81 8:1–28. https://doi.org/10.1186/S13756-019-0559-6
49. Khani R, Roostaei B, Bagherzade G, Moudi M (2018) Green synthesis of copper nanoparticles by fruit extract of Ziziphus spina-christi (L.) Willd.: Application for adsorption of triphenylmethane dye and antibacterial assay. J Mol Liq 255:541–549. https://doi.org/10.1016/J.MOLLIQ.2018.02.010
50. Lagergren S (1898) About the Theory of So-Called Adsorption of Soluble Substances. K- Sven Vetenskapsakademiens Handl 24:1–39
51. Langmuir I (1918) The adsorption of gases on plane surfaces of glass, mica and platinum. J Am Chem Soc 40:1361–1403. https://doi.org/10.1021/JA02242A004
52. Liu X, Lu S, Liu Y et al (2017) Adsorption of sulfamethoxazole (SMZ) and ciprofloxacin (CIP) by humic acid (HA): characteristics and mechanism. RSC Adv 7:50449–50458. https://doi.org/10.1039/C7RA06231A
53. Liu Y, Liu X, Lu S et al (2020a) Adsorption and biodegradation of sulfamethoxazole and ofloxacin on zeolite: Influence of particle diameter and redox potential. Chem Eng J 384:123346. https://doi.org/10.1016/J.CEJ.2019.123346
54. Liu Y, Peng Y, An B et al (2020b) Effect of molecular structure on the adsorption affinity of sulfonamides onto CNTs: Batch experiments and DFT calculations. Chemosphere 246:125778. https://doi.org/10.1016/J.CHEMOSPHERE.2019.125778
55. Lv M, Li D, Zhang Z et al (2021) Unveiling the correlation of Fe3O4 fractions upon the adsorption behavior of sulfamethoxazole on magnetic activated carbon. Sci Total Environ 757:143717. https://doi.org/10.1016/J.SCITOTENV.2020.143717

56. Marouzi S, Sabouri Z, Darroudi M (2021) Greener synthesis and medical applications of metal oxide nanoparticles. Ceram Int 47:19632–19650. https://doi.org/10.1016/J.CERAMINT.2021.03.301
57. Mitchell SM, Ullman JL, Teel AL, Watts RJ (2014) pH and temperature effects on the hydrolysis of three β-lactam antibiotics: Ampicillin, cefalotin and cefoxitin. Sci Total Environ 466–467:547–555. https://doi.org/10.1016/J.SCITOTENV.2013.06.027
58. Mohammadi M, Hekmatara SH, Moghaddam RS, Darehkordi A (2019) Preparation and optimization photocatalytic activity of polymer-grafted Ag@AgO core-shell quantum dots. Environ Sci Pollut Res 2019 2613 26:13401–13409. https://doi.org/10.1007/S11356-019-04685-2
59. Mourid EH, Lakraimi M, Benaziz L et al (2019) Wastewater treatment test by removal of the sulfamethoxazole antibiotic by a calcined layered double hydroxide. Appl Clay Sci 168:87–95. https://doi.org/10.1016/J.CLAY.2018.11.005
60. Obot IB, Obi-Egbedi NO (2010) Theoretical study of benzimidazole and its derivatives and their potential activity as corrosion inhibitors. Corros Sci 52:657–660. https://doi.org/10.1016/J.CORSCI.2009.10.017
61. Ogunleye DT, Akpotu SO, Moodley B (2020) Adsorption of sulfamethoxazole and reactive blue 19 using graphene oxide modified with imidazolium based ionic liquid. Environ Technol Innov 17:100616. https://doi.org/10.1016/J.ETI.2020.100616
62. Pai S, Kini SM, Narasimhan MK et al (2021) Structural characterization and adsorptive ability of green synthesized Fe3O4 nanoparticles to remove Acid blue 113 dye. Surf Interfaces 23:100947. https://doi.org/10.1016/J.SURFIN.2021.100947
63. Rashmi BN, Harlapur SF, Avinash B et al (2020) Facile green synthesis of silver oxide nanoparticles and their electrochemical, photocatalytic and biological studies. Inorg Chem Commun 111:107580. https://doi.org/10.1016/J.INOCHE.2019.107580
64. Reis AC, Kolvenbach BA, Nunes OC, Corvini PFX (2020) Biodegradation of antibiotics: The new resistance determinants – part I. N Biotechnol 54:34–51. https://doi.org/10.1016/J.NBT.2019.08.002
65. Serna-Carrizales JC, Collins-Martínez VH, Flórez E et al (2021) Adsorption of sulfamethoxazole, sulfadiazine and sulfametazine in single and ternary systems on activated carbon. Experimental and DFT computations. J Mol Liq 324:114740. https://doi.org/10.1016/J.MOLLIQ.2020.114740
66. Shamaila S, Sajjad AKL, Ryma N, ul A et al (2016) Advancements in nanoparticle fabrication by hazard free eco-friendly green routes. Appl Mater Today 5:150–199. https://doi.org/10.1016/J.APMT.2016.09.009
67. SI A, Pal K, Kralj S et al (2020) Sustainable preparation of gold nanoparticles via green chemistry approach for biogenic applications. Mater Today Chem 17:100327. https://doi.org/10.1016/J.MTCHEM.2020.100327
68. Stan M, Lung I, Soran ML et al (2017) Removal of antibiotics from aqueous solutions by green synthesized magnetite nanoparticles with selected agro-waste extracts. Process Saf Environ Prot 107:357–372. https://doi.org/10.1016/J.PSEP.2017.03.003

69. Stephens PJ, Devlin FJ, Chabalowski CF, Frisch MJ (1994) Ab Initio Calculation of Vibrational Absorption and Circular Dichroism Spectra Using Density Functional Force Fields. J Phys Chem 98:11623–11627. https://doi.org/10.1021/J100096A001
70. Straub JO, Hoffmann- F, Roche L (2016) Aquatic environmental risk assessment for human use of the old antibiotic sulfamethoxazole in Europe. Environ Toxicol Chem 35:767–779. https://doi.org/10.1002/ETC.2945
71. Suzuki S, Hoa PTP (2012) Distribution of quinolones, sulfonamides, tetracyclines in aquatic environment and antibiotic resistance in Indochina. Front Microbiol 3:67. https://doi.org/10.3389/FMICB.2012.00067/BIBTEX
72. Taher T, Putra R, Rahayu Palapa N, Lesbani A (2021) Preparation of magnetite-nanoparticle-decorated NiFe layered double hydroxide and its adsorption performance for congo red dye removal. Chem Phys Lett 777:138712. https://doi.org/10.1016/J.CPLETT.2021.138712
73. Tavlieva MP, Genieva SD, Georgieva VG, Vlaev LT (2013) Kinetic study of brilliant green adsorption from aqueous solution onto white rice husk ash. J Colloid Interface Sci 409:112–122. https://doi.org/10.1016/J.JCIS.2013.07.052
74. Wang F, Sun W, Pan W, Xu N (2015) Adsorption of sulfamethoxazole and 17β-estradiol by carbon nanotubes/CoFe2O4 composites. Chem Eng J 274:17–29. https://doi.org/10.1016/J.CEJ.2015.03.113
75. Wang P, Zhang D, Zhang H et al (2017) Impact of concentration and species of sulfamethoxazole and ofloxacin on their adsorption kinetics on sediments. Chemosphere 175:123–129. https://doi.org/10.1016/J.CHEMOSPHERE.2017.02.038
76. Wang T, Zhou Y, Cao S et al (2019) Degradation of sulfanilamide by Fenton-like reaction and optimization using response surface methodology. Ecotoxicol Environ Saf 172:334–340. https://doi.org/10.1016/J.ECOENV.2019.01.106
77. Wu M, Zhao S, Tang M et al (2019) Adsorption of sulfamethoxazole and tetracycline on montmorillonite in single and binary systems. Colloids Surf Physicochem Eng Asp 575:264–270. https://doi.org/10.1016/J.COLSURFA.2019.05.025
78. Wu S, Lin Y, Hu YH (2021) Strategies of tuning catalysts for efficient photodegradation of antibiotics in water environments: a review. J Mater Chem A 9:2592–2611. https://doi.org/10.1039/D0TA09173A
79. Xu D, Xie Y, Li J (2022) Toxic effects and molecular mechanisms of sulfamethoxazole on Scenedesmus obliquus. Ecotoxicol Environ Saf 232:113258. https://doi.org/10.1016/J.ECOENV.2022.113258
80. Xu L, Wei B, Liu W et al (2013a) Flower-like ZnO-Ag2O composites: Precipitation synthesis and photocatalytic activity. Nanoscale Res Lett 8:1–7. https://doi.org/10.1186/1556-276X-8-536/FIGURES/6
81. Xu M, Han L, Dong S (2013b) Facile fabrication of highly efficient g-C3N4/Ag 2O heterostructured photocatalysts with enhanced visible-light photocatalytic activity. ACS Appl Mater Interfaces

5:12533–12540. https://doi.org/10.1021/AM4038307/SUPPL_FILE/AM4038307_SI_001.PDF

82. Yao C, Chen T (2017) A film-diffusion-based adsorption kinetic equation and its application. Chem Eng Res Des 119:87–92. https://doi.org/10.1016/J.CHERD.2017.01.004
83. Yin F, Lin S, Zhou X et al (2021) Fate of antibiotics during membrane separation followed by physical-chemical treatment processes. Sci Total Environ 759:143520. https://doi.org/10.1016/J.SCITOTENV.2020.143520
84. Zamanpour N, Mohammad Esmaeily A, Mashreghi M et al (2021) Application of a marine luminescent Vibrio sp. B4L for biosynthesis of silver nanoparticles with unique characteristics, biochemical properties, antibacterial and antibiofilm activities. Bioorg Chem 114:105102. https://doi.org/10.1016/J.BIOORG.2021.105102
85. Zhang D, Pan B, Wu M et al (2011) Adsorption of sulfamethoxazole on functionalized carbon nanotubes as affected by cations and anions. Environ Pollut 159:2616–2621. https://doi.org/10.1016/J.ENVPOL.2011.05.036
86. Zhang D, Pan B, Zhang H et al (2010) Contribution of different sulfamethoxazole species to their overall adsorption on functionalized carbon nanotubes. Environ Sci Technol 44:3806–3811. https://doi.org/10.1021/ES903851Q/SUPPL_FILE/ES903851Q_SI_001.PDF
87. Zhang R, Zheng X, Chen B et al (2020) Enhanced adsorption of sulfamethoxazole from aqueous solution by Fe-impregnated graphited biochar. J Clean Prod 256:120662. https://doi.org/10.1016/J.JCLEPRO.2020.120662
88. Zhuang S, Chen R, Liu Y, Wang J (2020) Magnetic COFs for the adsorptive removal of diclofenac and sulfamethazine from aqueous solution: Adsorption kinetics, isotherms study and DFT calculation. J Hazard Mater 385:121596. https://doi.org/10.1016/J.JHAZMAT.2019.121596

Figures

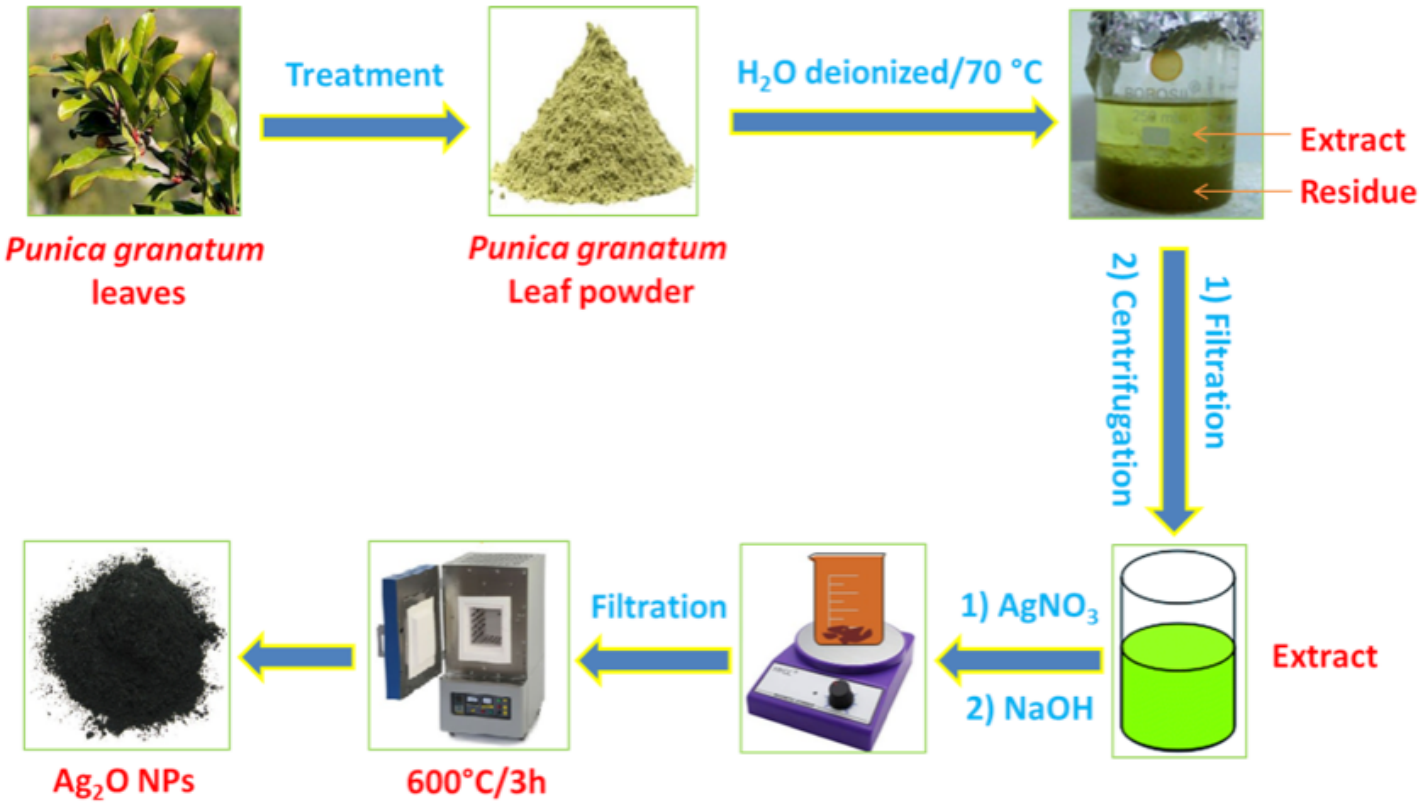

Figure 1

Green synthesis procedure of Ag_2O NPs from *Punica granatum* leaf extract.

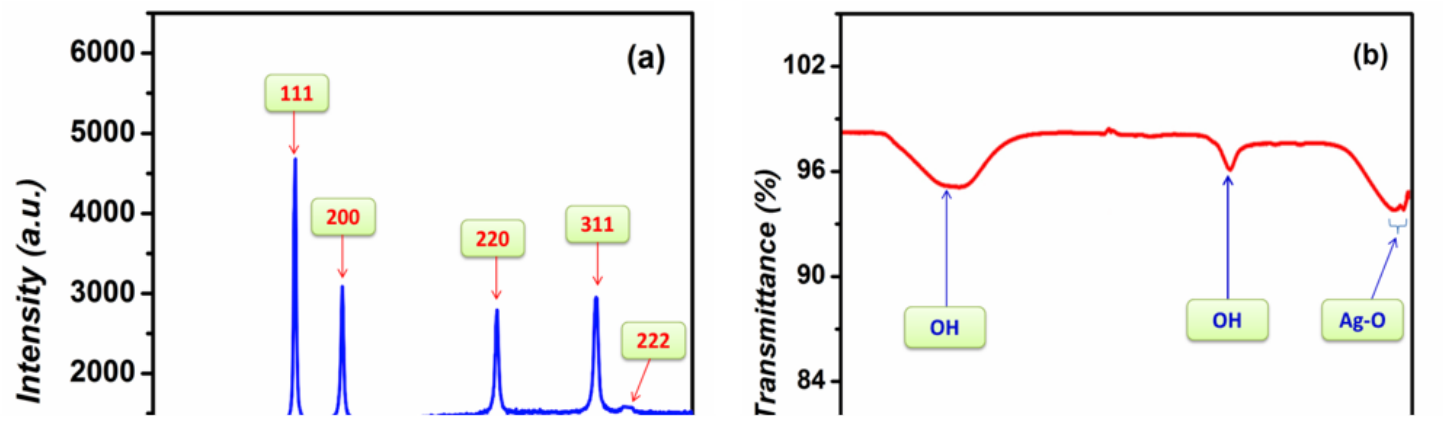

Figure 2

XRD (**a**) and FTIR (**b**) analysis, and N_2 adsorption/desorption isotherms

(included pore distribution) (**c**) of Ag_2O NPs.

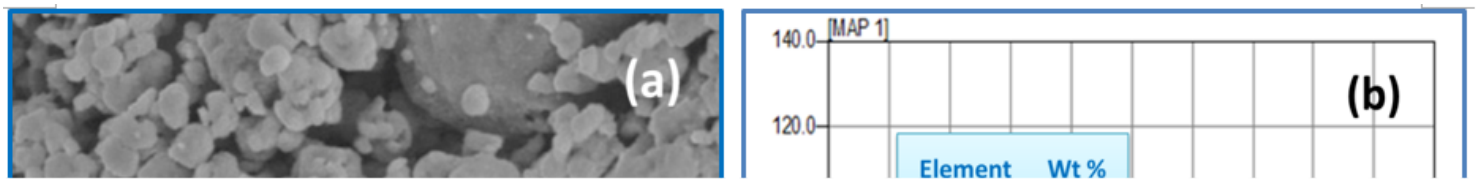

Figure 3

SEM micrograph (**a**), EDX elemental spectra (**b**), and TEM image (**c**) of Ag_2O NPs.

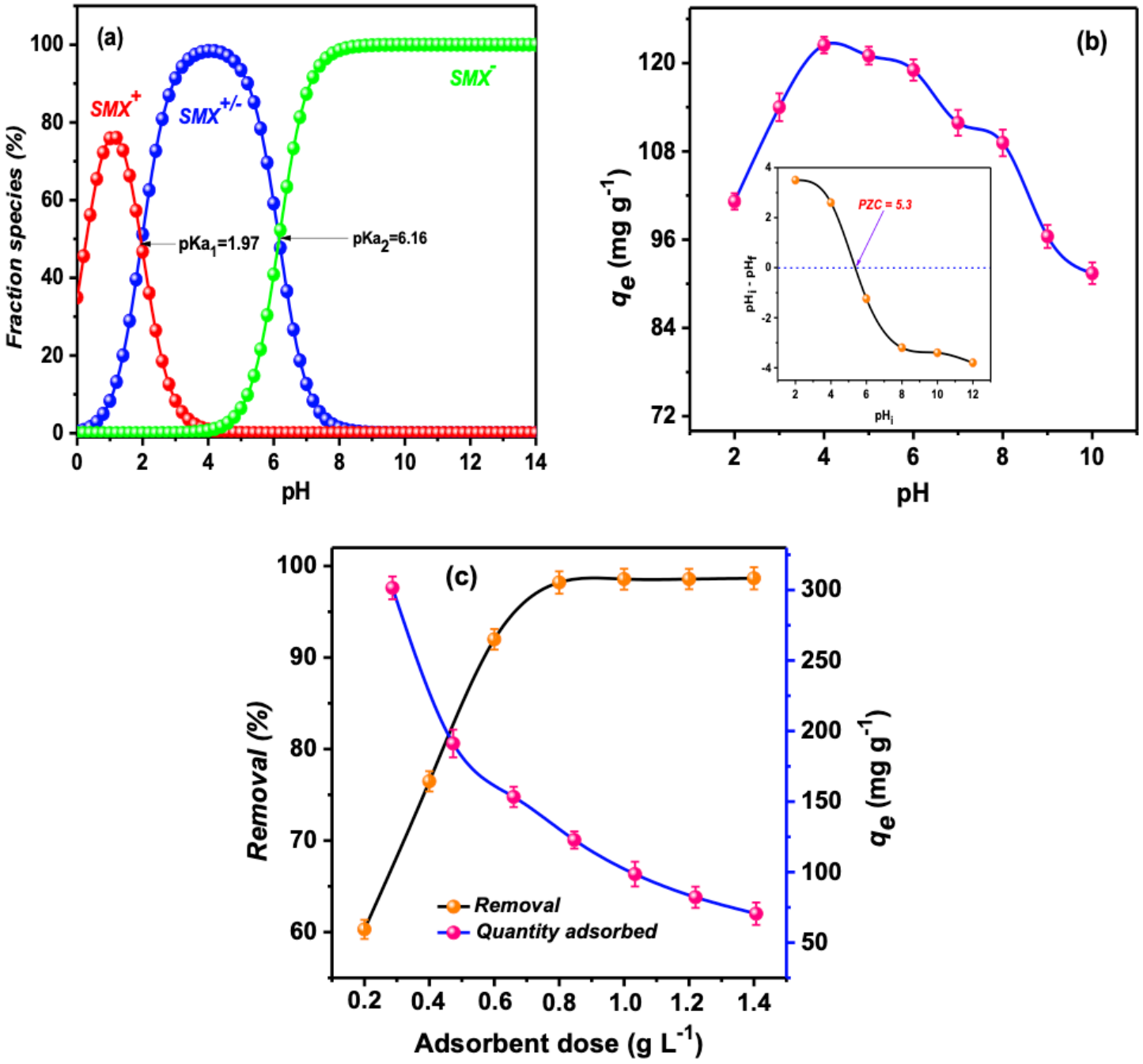

Figure 4

Distribution of the SMX species (**a**), Effects of pH of the solution (included PZC determination of Ag_2O NPs) (**b**), and adsorbent dose (**c**) on SMX adsorption.

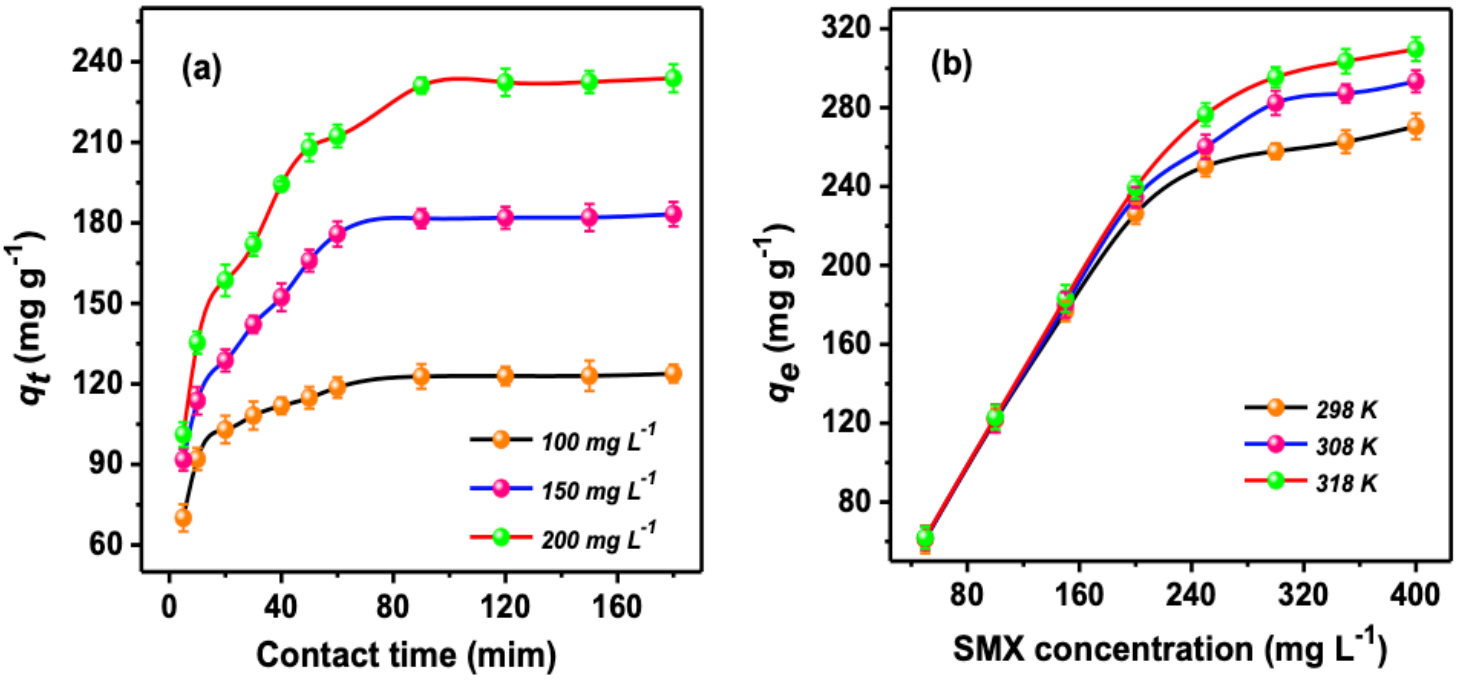

Figure 5

Effects of contact time at different SMX concentrations (**a**) and SMX concentration at different temperatures (**b**) on SMX adsorption.

Figure 6

Linearized PFO (**a**), PSO (**b**), and IPD (**c**) kinetic models for SMX adsorption on Ag_2O NPs.

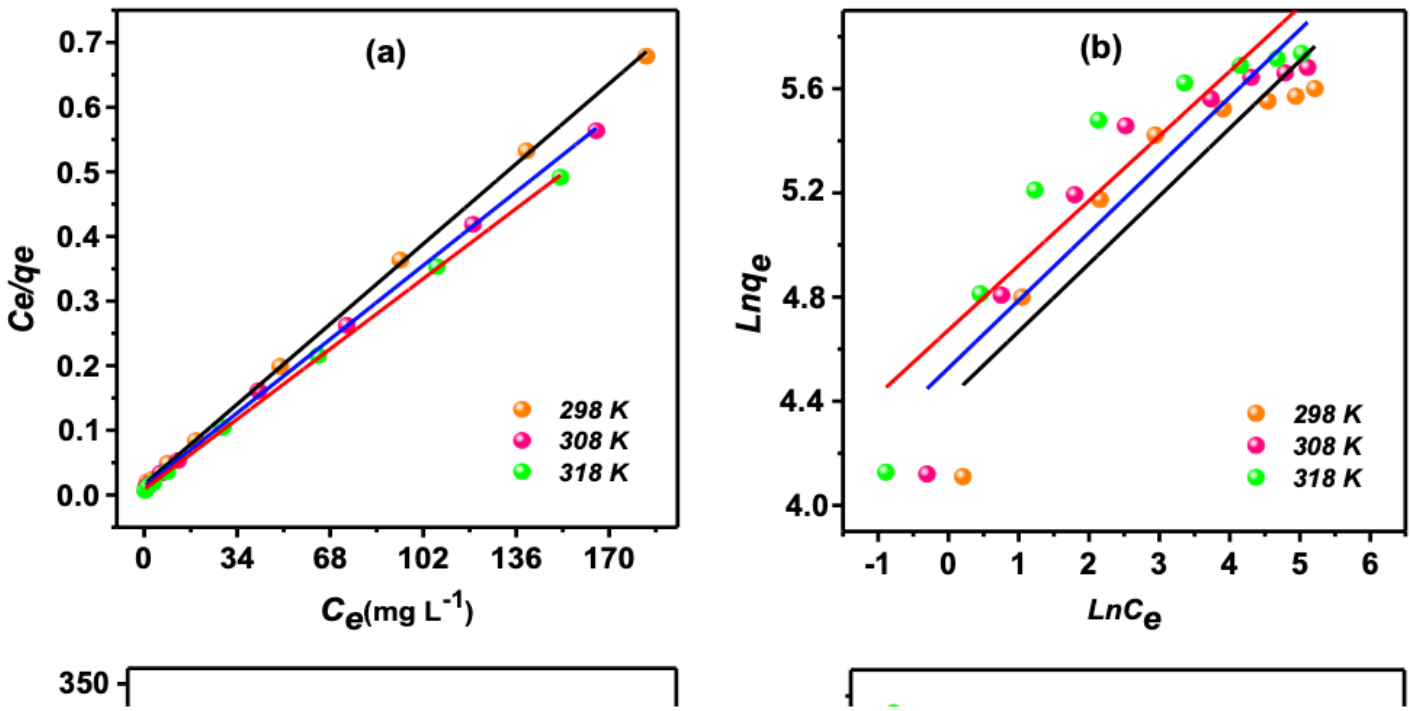

Figure 7

Linearized Langmuir (**a**), Freundlich (**b**), Temkin (**c**), and D-R (**d**) isotherm plots for SMX adsorption on Ag_2O NPs.

Figure 8

Van't Hoff plots for SMX adsorption on Ag_2O NPs (**a**) and recyclability of Ag_2O NPs for the SMX removal (**b**).

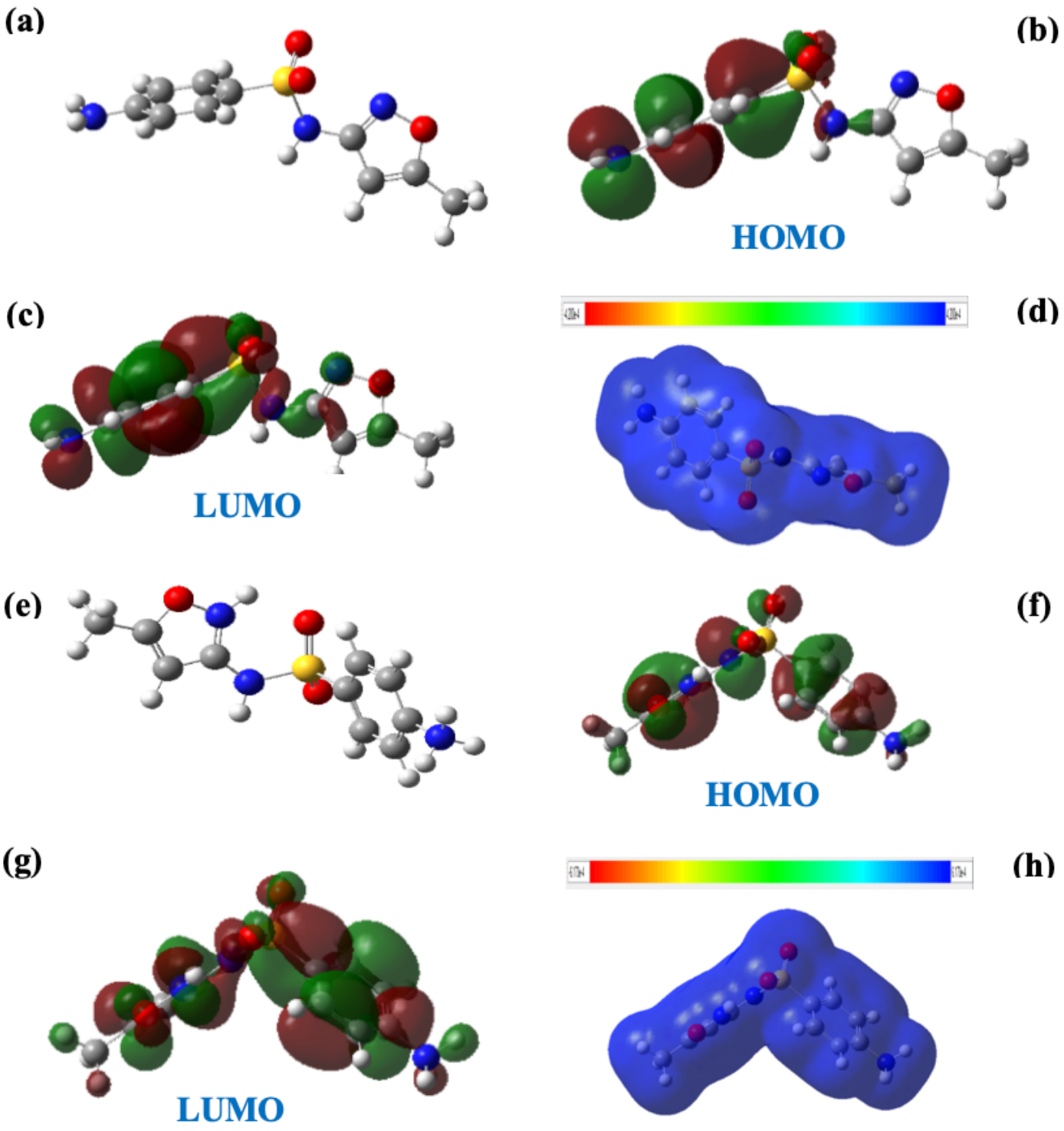

Figure 9

Optimized geometries, HOMO, LUMO frontier orbitals, and ESP (red, blue, yellow, and green: strongly negative, strongly positive, moderately negative, and moderately positive electrostatic potentials, respectively) maps for the $SMX^{+/-}$ (**a-d**) and SMX^{+} (**e-h**), respectively.

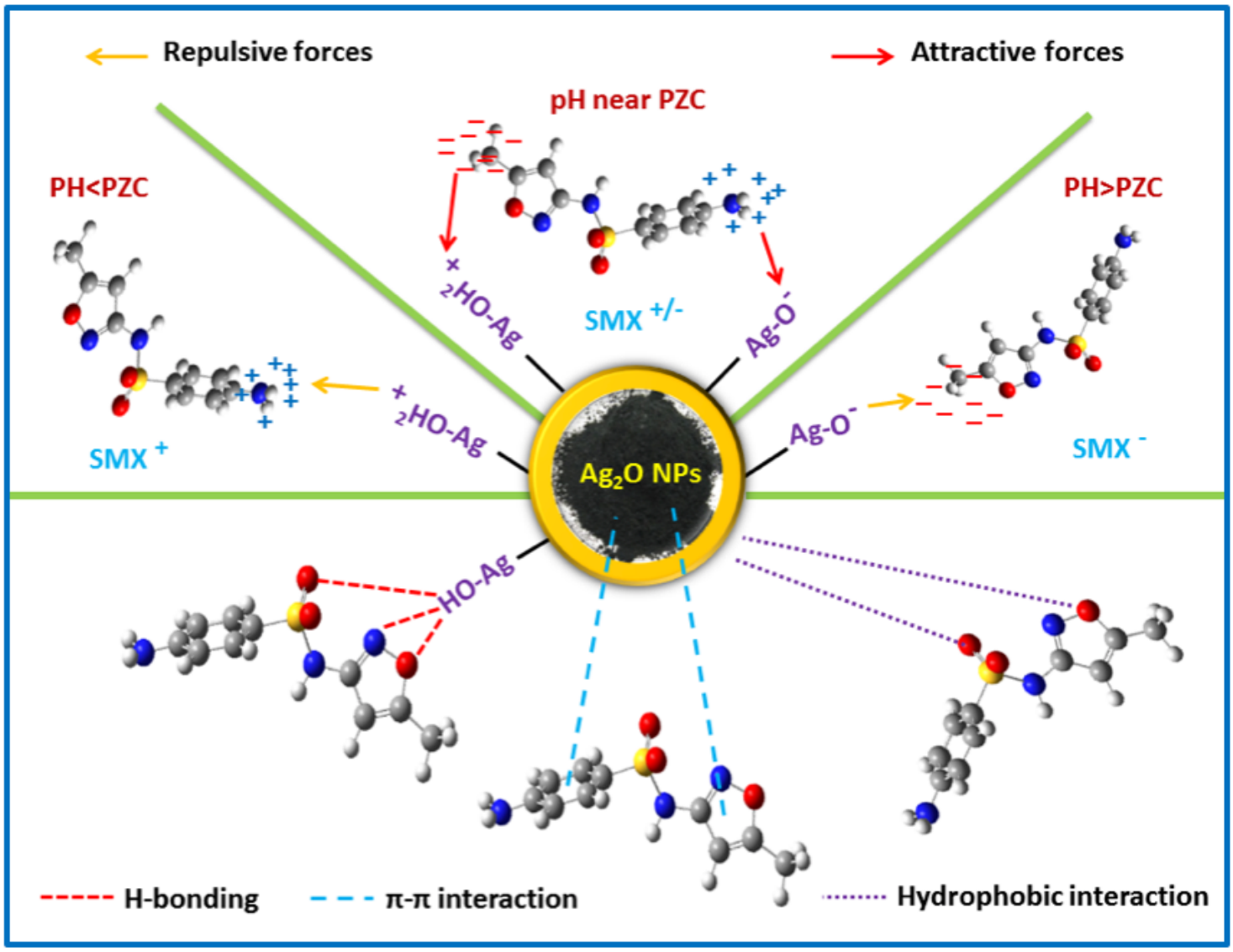

Figure 10

Proposed binding mechanism of the SMX on Ag_2O NPs.